

AN EFFICIENT SOLVER TO HELMHOLTZ EQUATIONS BY RECONSTRUCTION DISCONTINUOUS APPROXIMATION

SHUHAI ZHAO

ABSTRACT. In this paper, an efficient solver for the Helmholtz equation using a novel approximation space is developed. The ingredients of the method include the approximation space recently proposed, a discontinuous Galerkin scheme extensively used, and a linear system solver with a natural preconditioner. Comparing to traditional discontinuous Galerkin methods, we refer to the new method as being more efficient in the following sense. The numerical performance of the new method shows that: 1) much less error can be reached using the same degrees of freedom; 2) the sparse matrix therein has much fewer nonzero entries so that both the storage space and the solution time cost for the iterative solver are reduced; 3) the preconditioner is proved to be optimal with respect to the mesh size in the absorbing case. Such advantage becomes more pronounced as the approximation order increases.

keywords: Helmholtz problem, reconstructed discontinuous approximation, preconditioner.

1. INTRODUCTION

The Helmholtz equation, derived as the frequency-domain reduction of the wave equation, governs time-harmonic wave propagation in heterogeneous media. It serves as a fundamental model across numerous scientific and engineering disciplines, including seismic imaging, radar scattering, acoustic design, and photonic crystal modeling [25, 14, 5, 24]. The equation captures essential physical phenomena such as wave diffraction, interference, and dispersion, making its accurate numerical solution crucial for practical applications.

The highly oscillatory nature of Helmholtz solutions presents significant computational challenges, particularly in high-frequency regimes. Numerical resolution typically requires 6-10 grid points per wavelength, leading to extremely large linear systems when modeling realistic problems. These discretized systems yield sparse matrices that are not only large-scale but also inherently ill-conditioned and indefinite due to the presence of both elliptic and negative mass terms. The combination of these factors makes the Helmholtz equation considerably more difficult to solve numerically compared to standard elliptic partial differential equations.

The development of efficient numerical methods for Helmholtz problems has been an active research area for decades. Early work focused on conforming finite element methods [16, 17, 23], which provide rigorous error analysis but face challenges in handling complex geometries and achieving high-order accuracy. More recently, discontinuous Galerkin (DG) methods have gained popularity due to their flexibility in mesh handling, natural accommodation of hanging nodes, and ease of implementing high-order approximations [6, 7, 1, 13]. However, conventional DG methods typically require multiple degrees of freedom per element, leading to increased computational costs and memory requirements.

The design of effective preconditioners for Helmholtz problems represents another major research thrust. Traditional preconditioning strategies often struggle with the indefinite nature of the problem. Notable approaches include complex-shifted Laplacian preconditioners [3, 4, 8], which transform the indefinite problem into a nearby definite one, and domain decomposition methods [11, 12, 9, 10], which exploit local solves to construct effective preconditioners. Despite these advances, developing robust and scalable preconditioners for Helmholtz problems remains challenging.

In this paper, we apply the reconstructed discontinuous approximation (RDA) method [20, 19, 21, 18] to the Helmholtz problem. The construction of the finite element approximation space includes creating an element patch for each element and solving local least squares problems to obtain the basis functions. A distinctive feature of the RDA method is that it maintains only a single degree of freedom per element, significantly reducing the total number of degrees of freedom compared to conventional DG methods while preserving high-order accuracy. This efficiency gain translates to reduced memory requirements and computational costs. We demonstrate through numerical experiments that the RDA method achieves substantially smaller L^2 errors compared to standard DG methods with equivalent numbers of degrees of freedom. Also, we show that the resulting stiffness matrices contain significantly fewer non-zero entries than their DG counterparts while maintaining comparable accuracy. What's more, we develop a novel preconditioning strategy that leverages the structure of the RDA spaces that the degrees of freedom is independent of the reconstruction order, from which we construct a natural preconditioner from the piecewise constant space to any high-order reconstructed space. We establish convergence properties of the resulting non-Hermitian complex linear system within the framework of standard GMRES convergence theory and propose a specialized geometric multigrid algorithm for efficiently solving the preconditioned system. The numerical experiments presented in this work systematically validate the effectiveness of our approach. Comparative studies with conventional DG methods demonstrate superior performance in terms of both accuracy and computational efficiency.

The rest of this paper is organized as follows. In Section 2, we introduce the RDA finite element space and provide the necessary background on Sobolev spaces and mesh partitioning. Fundamental properties of the reconstruction operator are established. In Section 4, we describe the numerical scheme for the Helmholtz problem, introduce our preconditioning strategy, and present the main theoretical results. Section 5 contains comprehensive numerical experiments validating our theoretical findings and demonstrating the efficiency of our method. Finally, we offer concluding remarks in Section 6.

2. PRELIMINARIES

Let $\Omega \subset \mathbb{R}^d$ (with $d = 2, 3$) be a bounded polygonal (or polyhedral) domain with a Lipschitz boundary $\partial\Omega$. We begin by introducing some basic notation.

Let \mathcal{T}_h be a quasi-uniform mesh partition of Ω into disjoint open triangles (or tetrahedra). Denote by \mathcal{E}_h the set of all $(d-1)$ -dimensional faces of \mathcal{T}_h , and decompose it as $\mathcal{E}_h = \mathcal{E}_h^i \cup \mathcal{E}_h^b$, where \mathcal{E}_h^i and \mathcal{E}_h^b are the sets of interior and boundary faces, respectively. Define

$$h_K := \text{diam}(K), \quad \forall K \in \mathcal{T}_h, \quad h_e := \text{diam}(e), \quad \forall e \in \mathcal{E}_h,$$

and set $h := \max_{K \in \mathcal{T}_h} h_K$. The quasi-uniformity of \mathcal{T}_h means there exists a constant $\nu > 0$ such that $h \leq \nu \min_{K \in \mathcal{T}_h} \rho_K$, where ρ_K is the diameter of the largest ball inscribed in K . For a subdomain $D \subset \Omega$, we use the standard notations $L^2(D)$ and $H^s(D)$ for the complex-valued Sobolev spaces with $s \geq 0$; their corresponding semi-norms and norms are induced by the complex L^2 inner product.

The Helmholtz equation is given by

$$(1) \quad \begin{cases} -\Delta u - k^2 u = f, & \text{in } \Omega, \\ \frac{\partial u}{\partial \mathbf{n}} + ik u = g, & \text{on } \partial\Omega, \end{cases}$$

where k is the wavenumber, $i = \sqrt{-1}$ is the imaginary unit, and \mathbf{n} denotes the unit outward normal to Ω . In this paper, we also consider the Helmholtz equation with absorption ($\epsilon > 0$) [22, 8]:

$$(2) \quad \begin{cases} -\Delta u - (k^2 - i\epsilon) u = f, & \text{in } \Omega, \\ \frac{\partial u}{\partial \mathbf{n}} + ik u = g, & \text{on } \partial\Omega. \end{cases}$$

We recall the following regularity result, proved in [8].

Theorem 1. *Let $\Omega \subset \mathbb{R}^d$ be a smooth domain that is star-shaped with respect to a ball. Assume the coefficient satisfies $\epsilon \lesssim k^2$, and let $f \in L^2(\Omega)$, $g \in H^{1/2}(\partial\Omega)$. Then the solution u to the Helmholtz problem belongs to $H^2(\Omega)$. Moreover, there exists a constant C such that*

$$(3) \quad \|u\|_{H^2(\Omega)} \leq C(1 + k) \left(\|f\|_{L^2(\Omega)} + \|g\|_{H^{1/2}(\partial\Omega)} \right).$$

We also introduce the trace operators that will be used in our numerical schemes. For any piecewise smooth scalar-valued function v and vector-valued function $\boldsymbol{\tau}$, the jump operator $[\cdot]$ and the average operator $\{\cdot\}$ are defined on interior faces $e \in \mathcal{E}_h^i$ by

$$\begin{aligned} [v]|_e &:= v^+|_e - v^-|_e, & \{v\}|_e &:= \frac{1}{2}(v^+|_e + v^-|_e), \\ [\boldsymbol{\tau}]|_e &:= \boldsymbol{\tau}^+|_e - \boldsymbol{\tau}^-|_e, & \{\boldsymbol{\tau}\}|_e &:= \frac{1}{2}(\boldsymbol{\tau}^+|_e + \boldsymbol{\tau}^-|_e), \end{aligned}$$

where $v^\pm := v|_{K^\pm}$ and $\boldsymbol{\tau}^\pm := \boldsymbol{\tau}|_{K^\pm}$. On a boundary face $e \in \mathcal{E}_h^b$, these operators are modified as

$$\begin{aligned} [v]|_e &:= v|_e, & \{v\}|_e &:= v|_e, \\ [\boldsymbol{\tau}]|_e &:= \boldsymbol{\tau}|_e, & \{\boldsymbol{\tau}\}|_e &:= \boldsymbol{\tau}|_e, \end{aligned}$$

where \mathbf{n} is the unit outward normal to e .

Throughout the paper, the letters C and C with subscripts denote generic constants that may change from line to line but are independent of the mesh size.

3. RECONSTRUCTED DISCONTINUOUS SPACE

This section provides a brief introduction to the RDA (Reconstructed Discontinuous Approximation) finite element space. For proofs of the lemmas and theorems, we refer the reader to [18].

The definition of the RDA space relies on a carefully designed linear reconstruction operator that maintains high-order approximation properties while preserving the original degrees of freedom. The reconstruction procedure involves local polynomial fitting on a neighborhood patch for each element. The key steps are as follows.

For any element $K \in \mathcal{T}_h$, we construct an element patch $S(K)$ consisting of K itself and some surrounding elements. We use a recursive algorithm: for an element K , define $S_t(K)$ for $t = 0, 1, \dots$ by

$$(4) \quad S_0(K) = \{K\}, \quad S_t(K) = \bigcup_{\tilde{K} \in \mathcal{T}_h, \partial\tilde{K} \cap \partial\tilde{K} \in \mathcal{E}_h, \tilde{K} \in S_{t-1}(K)} \tilde{K}, \quad t \geq 1.$$

The recursion stops when t satisfies $\#S_t(K) \geq \#S$, and we set $S(K) := S_t(K)$. This algorithm is applied to all elements in \mathcal{T}_h to determine the patches.

Let $I(K)$ be the set of collocation points located inside the patch $S(K)$,

$$I(K) := \left\{ \mathbf{x}_{\tilde{K}} \mid \tilde{K} \in S(K) \right\}.$$

Given a piecewise constant function $g \in U_h^0$, for every element $K \in \mathcal{T}_h$ we seek a polynomial $\mathcal{R}_K g$ of degree $m \geq 1$ defined on $S(K)$ by solving the constrained least-squares problem:

$$(5) \quad \begin{aligned} \mathcal{R}_K g &= \arg \min_{p \in \mathbb{P}^m(S(K))} \sum_{\mathbf{x} \in I(K)} |p(\mathbf{x}) - g(\mathbf{x})|^2, \\ &\text{subject to } p(\mathbf{x}_K) = g(\mathbf{x}_K). \end{aligned}$$

The existence and uniqueness of the solution to (5) depend on the geometric distribution of the points in $I(K)$. We make the following assumption [19]:

Assumption 1. *For any element $K \in \mathcal{T}_h$ and any polynomial $p \in \mathbb{P}^m(S(K))$,*

$$p|_{I(K)} = 0 \quad \text{implies} \quad p|_{S(K)} \equiv 0.$$

The global linear reconstruction operator \mathcal{R} is then defined piecewise by the local operators \mathcal{R}_K :

$$(6) \quad \mathcal{R}v_h|_K := \mathcal{R}_K v_h|_K, \quad \forall K \in \mathcal{T}_h.$$

Thus, \mathcal{R} maps the piecewise constant space U_h^0 onto a subspace of the m th-order piecewise polynomial space, which we denote by $U_h^m = \mathcal{R}U_h^0$. The reconstructed space U_h^m will serve as the approximation space in the next section.

Define the characteristic functions for the piecewise constant space U_h^0 :

$$e_K(\mathbf{x}) = \begin{cases} 1, & \mathbf{x} \in K, \\ 0, & \text{otherwise.} \end{cases}$$

These functions form a basis for U_h^0 . Let $\lambda_K = \mathcal{R}e_K$. The following lemma ensures that $\{\lambda_K\}$ is a basis for U_h^m .

Lemma 1. *The functions $\{\lambda_K\}$ are linearly independent, and U_h^m is spanned by $\{\lambda_K\}$.*

The action of \mathcal{R} on a continuous function can be expressed explicitly: for any $g(\mathbf{x}) \in C^{m+1}(\Omega)$,

$$(7) \quad \mathcal{R}g = \sum_{K \in \mathcal{T}_h} g(\mathbf{x}_K) \lambda_K(\mathbf{x}).$$

Finally, we state the following approximation estimates for the reconstruction operator [18], which are essential for proving error estimates.

Theorem 2. *For any element $K \in \mathcal{T}_h$ and any $g \in H^{m+1}(\Omega)$, the following estimate holds:*

$$(8) \quad \|g - \mathcal{R}g\|_{H^q(K)} \leq C \Lambda_m h_K^{m+1-q} \|g\|_{H^{m+1}(S(K))}, \quad 0 \leq q \leq m,$$

where

$$\Lambda(m, S(K)) := \max_{p \in \mathbb{P}_m(S(K))} \frac{\max_{\mathbf{x} \in S(K)} |p(\mathbf{x})|}{\max_{\mathbf{x} \in I(K)} |p(\mathbf{x})|}, \quad \Lambda_m := \max_{K \in \mathcal{T}_h} (1 + \Lambda(m, S(K))) \sqrt{\#S(K)}.$$

3.1. An Intuitive Analysis of Approximation Efficiency for 1D Reconstruction. As will be demonstrated in Section 5, a significant advantage of the RDA discretization is its ability to achieve smaller numerical error for the same number of degrees of freedom compared to traditional DG finite element spaces.

We first recall a standard result from interpolation theory.

Lemma 2. *Let $f \in C^{m+1}([a, b])$, and let $x_0, x_1, \dots, x_m \in [a, b]$ be distinct nodes. Denote by $Lf(x)$ the Lagrange interpolation polynomial of degree m through these nodes. Then for any $x \in [a, b]$, there exists $\xi_x \in (a, b)$ such that*

$$f(x) - Lf(x) = \frac{f^{(m+1)}(\xi_x)}{(m+1)!} \prod_{i=0}^m (x - x_i).$$

For simplicity, we assume $g \in C^{m+1}(\bar{\Omega})$. By the interpolation formula above, there exists a point ξ_x such that

$$g(x) - \mathcal{R}g(x) = \frac{g^{(m+1)}(\xi_x)}{(m+1)!} \omega(x),$$

where $\omega(x) = \prod_{i=0}^m (x - x_i)$. The L^2 error estimate for RDA interpolation on an element K is then

$$\|g - \mathcal{R}g\|_{L^2(K)} \leq \frac{\|g^{(m+1)}\|_{L^\infty}}{(m+1)!} \|\omega\|_{L^2(K)}.$$

Consider the case where $\#S(K) = m+1$, i.e., on a mesh with scale $h_{\text{DG}} = (m+1)h_{\text{RDA}}$, the RDA and DG methods employ the same number of degrees of freedom. Correspondingly, the error estimate for DG interpolation over the same number of DOFs is

$$\|g - Ig\|_{L^2(S(K))} \leq \frac{\|g^{(m+1)}\|_{L^\infty}}{(m+1)!} \|\omega\|_{L^2(S(K))}.$$

Let x_0 and x_m be the left and right endpoints of $S(K)$, and assume K is the central element of $S(K)$. In this setting, the Lagrange interpolation polynomial of DG over $S(K)$ coincides with that of RDA over K . Since the interpolation error expression for RDA is

identical on each element of $S(K)$ (the interpolation points are simply translated), we can compute the ratio of the L^2 error upper bounds for RDA and DG interpolation:

$$C_m = \left(\frac{\int_{x_0}^{x_m} \omega(x)^2 dx}{(m+1) \int_K \omega(x)^2 dx} \right)^{1/2}.$$

By a change of variable, this can be rewritten as

$$C_m = \left(\frac{\int_0^{m+1} \tilde{\omega}(x)^2 dx}{(m+1) \int_{[m/2]}^{[m/2]+1} \tilde{\omega}(x)^2 dx} \right)^{1/2},$$

where $\tilde{\omega}(x) = \prod_{i=0}^m (x - (i + \frac{1}{2}))$.

We perform a numerical test using the function $g(x) = \sin(20\pi x)$, with RDA mesh size $h_{\text{RDA}} = h/(m+1)$, and compute both the ratio of interpolation errors and the ratio of numerical solution errors obtained by the IPDG method.

m	Theoretical C_m	$\frac{\ g - \mathcal{R}g\ _{L^2}}{\ g - Ig\ _{L^2}}$	FEM Error Ratio
2	$\frac{1}{3} \sqrt{\frac{407}{263}} \approx 0.426$	0.417	0.452
3	$\sqrt{\frac{20219}{233579}} \approx 0.294$	0.295	0.319
4	$\frac{1}{13} \sqrt{\frac{128123}{36395}} \approx 0.144$	0.145	0.168
5	$\frac{1}{9} \sqrt{\frac{507316223}{783956623}} \approx 0.0894$	0.0897	0.116
6	$\sqrt{\frac{1067989595}{540028301771}} \approx 0.0445$	0.0446	0.0530

4. NUMERICAL ANALYSIS

We begin by proposing the RDA discretization for problem (2). Define

$$\begin{aligned} A_h(u, v) := & \sum_{K \in \mathcal{T}_h} \int_K \nabla u \cdot \bar{\nabla} v \, dx - \sum_{e \in \mathcal{E}_h^i} \int_e \left(\llbracket u \rrbracket \cdot \{\bar{\nabla} v\} + \llbracket \bar{v} \rrbracket \cdot \{\nabla u\} \right) \, ds \\ & + \sum_{e \in \mathcal{E}_h^i} i \int_e \mu \llbracket u \rrbracket \cdot \llbracket \bar{v} \rrbracket \, ds, \end{aligned}$$

where μ is the penalty parameter:

$$\mu = \frac{\eta}{h_e}, \quad \text{for } e \in \mathcal{E}_h.$$

Define also

$$a_h(u, v) := A_h(u, v) - \sum_{K \in \mathcal{T}_h} (k^2 - i\epsilon) \int_K u \bar{v} \, d\mathbf{x} + \sum_{e \in \mathcal{E}_h^b} \int_e ik u \bar{v} \, d\mathbf{s}.$$

The bilinear form is defined on the space $U_h := U_h^m + H^2(\Omega)$. The numerical scheme reads: find $u_h \in U_h^m$ such that

$$(9) \quad a_h(u_h, v_h) = l_h(v_h), \quad \forall v_h \in U_h^m,$$

where the linear form l_h for $v \in U_h$ is given by

$$l_h(v) := \sum_{K \in \mathcal{T}_h} \int_K f \bar{v} \, d\mathbf{x} + \sum_{e \in \mathcal{E}_h^b} \int_e g \bar{v} \, d\mathbf{s}.$$

For error analysis, we introduce the energy norms on U_h :

$$\|v\|_{\text{DG}}^2 := \sum_{K \in \mathcal{T}_h} \|\nabla v\|_{L^2(K)}^2 + \sum_{e \in \mathcal{E}_h^i} h_e^{-1} \|\llbracket v \rrbracket\|_{L^2(e)}^2 + \sum_{e \in \mathcal{E}_h^b} k \|v\|_{L^2(e)}^2,$$

and

$$\|v\|^2 := \|v\|_{\text{DG}}^2 + \sum_{e \in \mathcal{E}_h^i} h \|\{\nabla v\}\|_{L^2(e)}^2.$$

Note the following norm equivalence for $v_h \in U_h^m$:

$$\|v_h\|_{\text{DG}} \leq \|\llbracket v_h \rrbracket\| \leq C \|v_h\|_{\text{DG}}.$$

Lemma 3. *Let $u \in H^2(\Omega)$ be the solution to (2), and let $u_h \in U_h^m$ be the discrete solution to (9). Then*

$$(10) \quad a_h(u - u_h, v_h) = 0, \quad \forall v_h \in U_h^m.$$

Proof. First observe that, since u is continuous,

$$\llbracket u \rrbracket|_e = 0, \quad \forall e \in \mathcal{E}_h^i.$$

Substituting u into $a_h(\cdot, \cdot)$ yields

$$\begin{aligned} a_h(u, v_h) &= \sum_{K \in \mathcal{T}_h} \int_K \nabla u \cdot \bar{\nabla v_h} \, d\mathbf{x} - \sum_{K \in \mathcal{T}_h} \int_K (k^2 - i\epsilon) u \bar{v_h} \, d\mathbf{x} \\ &\quad - \sum_{e \in \mathcal{E}_h^i} \int_e \llbracket \bar{v_h} \rrbracket \cdot \{\nabla u\} \, d\mathbf{s} + \sum_{e \in \mathcal{E}_h^b} \int_e ik u \bar{v_h} \, d\mathbf{s}. \end{aligned}$$

Multiplying (2) by $\bar{v_h}$ and integrating by parts gives

$$\begin{aligned} \sum_{K \in \mathcal{T}_h} \int_K f \bar{v_h} \, d\mathbf{x} &= \sum_{K \in \mathcal{T}_h} \int_K \nabla u \cdot \bar{\nabla v_h} \, d\mathbf{x} - \sum_{K \in \mathcal{T}_h} \int_K (k^2 - i\epsilon) u \bar{v_h} \, d\mathbf{x} \\ &\quad - \sum_{e \in \mathcal{E}_h} \int_e \llbracket \bar{v_h} \rrbracket \cdot \{\nabla u\} \, d\mathbf{s}, \end{aligned}$$

where

$$\sum_{e \in \mathcal{E}_h} \int_e [\![\bar{v}_h]\!] \cdot \{\nabla u\} \, ds = \sum_{e \in \mathcal{E}_h^i} \int_e [\![\bar{v}_h]\!] \cdot \{\nabla u\} \, ds + \sum_{e \in \mathcal{E}_h^b} \int_e (g - ik u) \bar{v}_h \, ds.$$

Combining these identities, we obtain

$$a_h(u_h, v_h) = l_h(v_h) = a_h(u, v_h).$$

□

4.1. Elliptic Projection. A key technique for error analysis is the elliptic projection. For $u, w \in H^2(\Omega)$, define Pu and Qw by

$$\begin{aligned} A_h(Pu, v_h) + ik(Pu, v_h)_{L^2(\partial\Omega)} &= A_h(u, v_h) + ik(u, v_h)_{L^2(\partial\Omega)}, \quad \forall v_h \in U_h^m, \\ A_h(v_h, Qw) + ik(v_h, Qw)_{L^2(\partial\Omega)} &= A_h(v_h, w) + ik(v_h, w)_{L^2(\partial\Omega)}, \quad \forall v_h \in U_h^m. \end{aligned}$$

Since Pu and Qw are solutions to elliptic problems with data u and w , respectively, the following error estimates hold [2]:

Lemma 4. *Assuming $hk \lesssim 1$, we have*

$$\begin{aligned} \|[u - Pu]\| &\leq \inf_{v \in U_h^m} \|[u - v]\|, & \|[w - Qw]\| &\leq \inf_{v \in U_h^m} \|[w - v]\|, \\ \|u - Pu\|_{L^2(\Omega)} &\leq h \inf_{v \in U_h^m} \|[u - v]\|, & \|w - Qw\|_{L^2(\Omega)} &\leq h \inf_{v \in U_h^m} \|[w - v]\|. \end{aligned}$$

4.2. Error Analysis.

Theorem 3. *The bilinear form a_h satisfies the boundedness condition:*

$$(11) \quad |a_h(u_h, v_h)| \leq C \|[u_h]\| \|[v_h]\|, \quad \forall u_h, v_h \in U_h.$$

Theorem 4. *For sufficiently large η , there holds*

$$(12) \quad |a_h(v_h, v_h)| \geq C \|[v_h]\|^2 - k^2 \|v_h\|_{L^2(\Omega)}^2, \quad \forall v_h \in U_h^m.$$

Proof. First note that

$$(13) \quad - \sum_{e \in \mathcal{E}_h^i} \int_e 2[\![v_h]\!] \cdot \{\nabla v_h\} \, ds \geq - \sum_{e \in \mathcal{E}_h^i} \frac{1}{\beta} \|h_e^{-1/2} [\![v_h]\!]\|_{L^2(e)}^2 - C\beta \sum_{K \in \mathcal{T}_h} \|\nabla v_h\|_{L^2(K)}^2,$$

for any $\beta > 0$. By the Cauchy-Schwarz inequality,

$$- \int_e 2[\![v_h]\!] \cdot \{\nabla v_h\} \, ds \geq - \frac{1}{\beta} \|h_e^{-1/2} [\![v_h]\!]\|_{L^2(e)}^2 - \beta \|h_e^{1/2} \{\nabla v_h\}\|_{L^2(e)}^2,$$

and by the inverse estimate (with $e = \partial K^+ \cap \partial K^-$)

$$\|h_e^{1/2} \nabla v_h\|_{L^2(e)} \leq C \|\nabla v_h\|_{L^2(K^+ \cup K^-)},$$

we obtain

$$\begin{aligned} & \sum_{K \in \mathcal{T}_h} \|\nabla v_h\|_{L^2(K)}^2 - 2 \sum_{e \in \mathcal{E}_h^i} \Re \int_e [\![v_h]\!] \cdot \{\bar{\nabla} v_h\} \, ds + \sum_{e \in \mathcal{E}_h^i} \mu \|[v_h]\|_{L^2(e)}^2 \\ & \geq (1 - C\beta) \sum_{K \in \mathcal{T}_h} \|\nabla v_h\|_{L^2(K)}^2 + \left(\eta - \frac{1}{\beta} \right) \sum_{e \in \mathcal{E}_h} \|h_e^{-1/2} [\![v_h]\!]\|_{L^2(e)}^2. \end{aligned}$$

Choosing $\beta = 1/(2C)$ and η sufficiently large, and using

$$\begin{aligned} a_h(v_h, v_h) &= \sum_{K \in \mathcal{T}_h} \|\nabla v_h\|_{L^2(K)}^2 - 2 \sum_{e \in \mathcal{E}_h^i} \Re \int_e [\![v_h]\!] \cdot \{\bar{\nabla v_h}\} \, ds + \sum_{e \in \mathcal{E}_h^i} i\mu \|\![\![v_h]\!]\|_{L^2(e)}^2 \\ &\quad - \sum_{K \in \mathcal{T}_h} (k^2 - i\epsilon) \|v_h\|_{L^2(K)}^2 + \sum_{e \in \mathcal{E}_h^b} ik \|v_h\|_{L^2(e)}^2, \end{aligned}$$

we conclude

$$\|v_h\|_{\text{DG}}^2 \lesssim |a_h(v_h, v_h) + 2k^2(v_h, v_h)|.$$

□

The following lemma provides an interpolation error estimate in the $\|\cdot\|$ norm.

Lemma 5. *There exists a constant C such that*

$$(14) \quad \|\![\![v - \mathcal{R}v]\!]\| \leq C\Lambda_m(1 + k^2h^2)^{1/2}h^m\|v\|_{H^{m+1}(\Omega)}, \quad \forall v \in H^{m+1}(\Omega).$$

Proof. By Theorem 2,

$$\sum_{K \in \mathcal{T}_h} \|\nabla v - \nabla(\mathcal{R}v)\|_{L^2(K)}^2 \leq C\Lambda_m^2 h^{2m} \|v\|_{H^{m+1}(\Omega)}^2.$$

Similarly,

$$\sum_{K \in \mathcal{T}_h} k^2 \|v - \mathcal{R}v\|_{L^2(K)}^2 \leq C\Lambda_m^2 k^2 h^{2m+2} \|v\|_{H^{m+1}(\Omega)}^2,$$

and by trace and inverse inequalities,

$$\sum_{e \in \mathcal{E}_h^b} k \|v - \mathcal{R}v\|_{L^2(e)}^2 \leq C\Lambda_m^2 kh^{2m+1} \|v\|_{H^{m+1}(\Omega)}^2.$$

The remaining terms are estimated analogously. □

We introduce the adjoint problem

$$(15) \quad \begin{cases} -\Delta w - (k^2 - i\epsilon)w = u - u_h, & \text{in } \Omega, \\ \frac{\partial w}{\partial \mathbf{n}} + ikw = 0, & \text{on } \partial\Omega. \end{cases}$$

For the error analysis, we assume the following regularity for w :

$$(16) \quad \|w\|_{H^2(\Omega)} \leq (1 + k)\|u - u_h\|_{L^2(\Omega)}.$$

Theorem 5. *Assume the solution u to (2) satisfies $u \in H^{m+1}(\Omega)$. For a sufficiently large penalty η and under the condition $k^3h^2 \lesssim 1$, there exists a constant C such that*

$$(17) \quad \|\![\![u - u_h]\!]\| \leq C\Lambda_m(1 + k^2h^2)^{1/2}h^m\|u\|_{H^{m+1}(\Omega)}.$$

Proof. Taking the inner product of (15) with $u - u_h$ and conjugating gives

$$\begin{aligned}
 \|u - u_h\|_{L^2(\Omega)}^2 &= A_h(u - u_h, w) - (k^2 - i\epsilon)(u - u_h, w)_{L^2(\Omega)} + ik(u - u_h, w)_{L^2(\partial\Omega)} \\
 &= A_h(u - u_h, w - Qw) - (k^2 - i\epsilon)(u - u_h, w - Qw)_{L^2(\Omega)} \\
 &\quad + ik(u - u_h, w - Qw)_{L^2(\partial\Omega)} \\
 (18) \quad &= A_h(u - Pu, w - Qw) - (k^2 - i\epsilon)(u - u_h, w - Qw)_{L^2(\Omega)} \\
 &\quad + ik(u - Pu, w - Qw)_{L^2(\partial\Omega)} \\
 &\leq \|u - Pu\| \|w - Qw\| + k^2 \|u - u_h\|_{L^2(\Omega)} \|w - Qw\|_{L^2(\Omega)}.
 \end{aligned}$$

Using the properties of the elliptic projection,

$$\begin{aligned}
 \|w - Qw\| &\leq h(1 + k^2 h^2)^{1/2} \Lambda_m \|w\|_{H^2(\Omega)} \leq kh(1 + k^2 h^2)^{1/2} \Lambda_m \|u - u_h\|_{L^2(\Omega)}, \\
 \|w - Qw\|_{L^2(\Omega)} &\leq Ckh^2(1 + k^2 h^2)^{1/2} \Lambda_m \|u - u_h\|_{L^2(\Omega)}.
 \end{aligned}$$

Therefore,

$$\begin{aligned}
 \|u - u_h\|_{L^2(\Omega)}^2 &\leq \|u - Pu\| kh(1 + k^2 h^2)^{1/2} \Lambda_m \|u - u_h\|_{L^2(\Omega)} \\
 &\quad + k^3 h^2 (1 + k^2 h^2)^{1/2} \Lambda_m^2 \|u - u_h\|_{L^2(\Omega)}^2.
 \end{aligned}$$

If $k^3 h^2 \Lambda_m^2 < 1/2$, then

$$\|u - u_h\|_{L^2(\Omega)} \leq Ckh(1 + k^2 h^2)^{1/2} \Lambda_m \|u - Pu\|.$$

The result follows from Lemma 4. \square

Corollary 1. *Under the same assumptions as Theorem 5, there exists a constant C such that*

$$(19) \quad \|u - u_h\|_{L^2(\Omega)} \leq Ck\Lambda_m(1 + k^2 h^2)h^{m+1} \|u\|_{H^{m+1}(\Omega)}.$$

Proof. Taking $v_h = \mathcal{R}u - u_h$ and using Theorem 12, we obtain

$$\begin{aligned}
 C\|\mathcal{R}u - u_h\|^2 &\leq \|\mathcal{R}u - u_h\|_{\text{DG}}^2 \\
 &\leq |a_h(\mathcal{R}u - u_h, \mathcal{R}u - u_h) + k^2(\mathcal{R}u - u_h, \mathcal{R}u - u_h)| \\
 &= |a_h(\mathcal{R}u - u, \mathcal{R}u - u_h) + k^2(\mathcal{R}u - u_h, \mathcal{R}u - u_h)| \\
 &\leq |a_h(\mathcal{R}u - u, \mathcal{R}u - u_h)| + k^2|(\mathcal{R}u - u, \mathcal{R}u - u_h)| \\
 &\quad + k^2|(u - u_h, \mathcal{R}u - u_h)|.
 \end{aligned}$$

Hence,

$$\|\mathcal{R}u - u_h\|^2 \leq C_0\|\mathcal{R}u - u\| \|\mathcal{R}u - u_h\| + C_0k\|u - u_h\|_{L^2(\Omega)} \|\mathcal{R}u - u_h\|.$$

Applying (5) completes the proof. \square

4.3. Preconditioner. We now turn our attention to preconditioning. The matrix form of the system is

$$a_h(u_h, v_h) = l_h(v_h) \Rightarrow A_\epsilon \mathbf{x} = \mathbf{b},$$

where $A_\epsilon \in \mathbb{C}^{n_e \times n_e}$, $\mathbf{x}, \mathbf{b} \in \mathbb{C}^{n_e}$. Note that the matrix size is independent of the order m .

We choose a preconditioner based on the lowest-order discretization: P corresponds to the bilinear form $a_h^0(\cdot, \cdot)$ acting on $U_h^0 \times U_h^0$:

$$a_h^0(u_h, v_h) = \sum_{e \in \mathcal{E}_h^i} \int_e \eta h^{-1} [\![u_h]\!] \cdot [\![v_h]\!] \, ds + \sum_{K \in \mathcal{T}_h} \int_K k^2 u_h \bar{v}_h \, dx + \sum_{e \in \mathcal{E}_h^b} \int_e k u_h \bar{v}_h \, ds.$$

We consider Krylov subspace iterative methods for solving the preconditioned linear system. Since the system is non-positive-definite, we employ the preconditioned GMRES (PGMRES) method. We first establish the following lemma for the absorbing case ($\epsilon > 0$).

Lemma 6. *If $0 < \epsilon \lesssim k^2$, there exists $\alpha > 0$ such that*

$$|a_h(\mathcal{R}v_h, \mathcal{R}v_h)| \geq \alpha \frac{\epsilon}{k^2} \|\mathcal{R}v_h\|_{DG}^2, \quad \forall v_h \in U_h^0.$$

Proof. Let p, q be such that

$$k^2 - i\epsilon = (p - iq)^2,$$

which implies $p \sim k$, $q \sim \epsilon/k$, since $\epsilon \lesssim k^2$. We have

$$\begin{aligned} a_h(\mathcal{R}v_h, \mathcal{R}v_h) &= \sum_{K \in \mathcal{T}_h} \|\nabla \mathcal{R}v_h\|_{L^2(K)}^2 - 2 \sum_{e \in \mathcal{E}_h^i} \Re \int_e [\![\mathcal{R}v_h]\!] \cdot \{\bar{\nabla} \mathcal{R}v_h\} \, ds \\ &\quad + \sum_{e \in \mathcal{E}_h^i} i\mu \|\mathcal{R}v_h\|_{L^2(e)}^2 - \sum_{K \in \mathcal{T}_h} (k^2 - i\epsilon) \|\mathcal{R}v_h\|_{L^2(K)}^2 \\ &\quad + \sum_{e \in \mathcal{E}_h^b} ik \|\mathcal{R}v_h\|_{L^2(e)}^2. \end{aligned}$$

Then,

$$\begin{aligned} &\Im((p + iq)a_h(\mathcal{R}v_h, \mathcal{R}v_h)) \\ &= q \left(\sum_{K \in \mathcal{T}_h} \|\nabla \mathcal{R}v_h\|_{L^2(K)}^2 - 2 \sum_{e \in \mathcal{E}_h^i} \Re \int_e [\![\mathcal{R}v_h]\!] \cdot \{\bar{\nabla} \mathcal{R}v_h\} \, ds \right) \\ &\quad + \sum_{K \in \mathcal{T}_h} q(p^2 + q^2) \|\mathcal{R}v_h\|_{L^2(K)}^2 + \sum_{e \in \mathcal{E}_h^b} pk \|\mathcal{R}v_h\|_{L^2(e)}^2 + \sum_{e \in \mathcal{E}_h^i} \mu p \|\mathcal{R}v_h\|_{L^2(e)}^2. \end{aligned}$$

Consequently,

$$\begin{aligned} |a_h(\mathcal{R}v_h, \mathcal{R}v_h)| &\geq \frac{Cq}{\sqrt{p^2 + q^2}} \left(\sum_{K \in \mathcal{T}_h} \|\nabla \mathcal{R}v_h\|_{L^2(K)}^2 + \sum_{e \in \mathcal{E}_h^i} \mu \|\mathcal{R}v_h\|_{L^2(e)}^2 \right) \\ &\quad + \sum_{K \in \mathcal{T}_h} q \sqrt{p^2 + q^2} \|\mathcal{R}v_h\|_{L^2(K)}^2 + \sum_{e \in \mathcal{E}_h^b} \frac{pk}{\sqrt{p^2 + q^2}} \|\mathcal{R}v_h\|_{L^2(e)}^2 \\ &\geq \alpha \frac{\epsilon}{k^2} \|\mathcal{R}v_h\|_{DG}^2. \end{aligned}$$

□

The following norm equivalence is crucial for the convergence of PGMRES.

Lemma 7. *Assume $hk \lesssim 1$. Then there exists a constant C independent of the mesh size such that*

$$(20) \quad \|v_h\|_{\text{DG}} \leq C\|\mathcal{R}v_h\|_{\text{DG}} \leq C\Lambda_m\|v_h\|_{\text{DG}}, \quad \forall v_h \in U_h^0.$$

Proof. We first prove the lower bound in (20). For the volume term, using the approximation property,

$$(21) \quad \|v_h - \mathcal{R}v_h\|_{L^2(K)} \leq Ch\|\nabla \mathcal{R}v_h\|_{L^2(K)},$$

hence

$$k^2\|v_h\|_{L^2(K)}^2 \leq k^2\|\mathcal{R}v_h\|_{L^2(K)}^2 + h^2k^2\|\nabla \mathcal{R}v_h\|_{L^2(K)}^2.$$

For an interior face $e \in \mathcal{E}_h^i$ with $e = \partial K_+ \cap \partial K_-$, let $v_{K^\pm} := v_h|_{K^\pm}$. By the constraint in (5), $v_{K^\pm} = I_{K^\pm}(\mathcal{R}_{K^\pm}v_h)$, where I_K denotes the constant interpolation at \mathbf{x}_K . Using inverse estimates,

$$\begin{aligned} h_e^{-1}\|\llbracket v_h \rrbracket\|_{L^2(e)}^2 &\leq Ch^{-1} \left(\|\mathcal{R}_{K^+}v_h - I_{K^+}\mathcal{R}_{K^+}v_h\|_{L^2(e)}^2 \right. \\ &\quad \left. + \|\mathcal{R}_{K^-}v_h - I_{K^-}\mathcal{R}_{K^-}v_h\|_{L^2(e)}^2 + \|\mathcal{R}_{K^+}v_h - \mathcal{R}_{K^-}v_h\|_{L^2(e)}^2 \right) \\ &\leq Ch^{-2} \left(\|\mathcal{R}_{K^+}v_h - I_{K^+}\mathcal{R}_{K^+}v_h\|_{L^2(K^+)}^2 \right. \\ &\quad \left. + \|\mathcal{R}_{K^-}v_h - I_{K^-}\mathcal{R}_{K^-}v_h\|_{L^2(K^-)}^2 + \|\mathcal{R}_{K^+}v_h - \mathcal{R}_{K^-}v_h\|_{L^2(e)}^2 \right) \\ &\leq C \left(\|\nabla \mathcal{R}_{K^+}v_h\|_{L^2(K^+)}^2 + \|\nabla \mathcal{R}_{K^-}v_h\|_{L^2(K^-)}^2 + h_e^{-1}\|\llbracket \mathcal{R}v_h \rrbracket\|_{L^2(e)}^2 \right). \end{aligned}$$

For a boundary face $e \in \mathcal{E}_h^b$ with $e \subset \partial K$, a similar estimate yields

$$\begin{aligned} h_e^{-1}\|v_h\|_{L^2(e)}^2 &\leq C \left(\|\nabla \mathcal{R}_K v_h\|_{L^2(K)}^2 + h_e^{-1}\|\llbracket \mathcal{R}_K v_h \rrbracket\|_{L^2(e)}^2 \right), \\ k\|v_h\|_{L^2(e)}^2 &\leq C \left(kh\|\nabla \mathcal{R}_K v_h\|_{L^2(K)}^2 + k\|\llbracket \mathcal{R}_K v_h \rrbracket\|_{L^2(e)}^2 \right). \end{aligned}$$

Summing over all faces and using $kh \lesssim 1$, we obtain $\|v_h\|_{\text{DG}} \leq C\|\mathcal{R}v_h\|_{\text{DG}}$.

For the upper bound, note that

$$k^2\|\mathcal{R}v_h\|_{L^2(K)}^2 \leq k^2\|v_h\|_{L^2(K)}^2 + h^2k^2\|\nabla \mathcal{R}v_h\|_{L^2(K)}^2.$$

For interior faces, using the same notation,

$$\begin{aligned} h_e^{-1}\|\llbracket \mathcal{R}v_h \rrbracket\|_{L^2(e)}^2 &\leq Ch_e^{-1} \left(\|\mathcal{R}_{K^+}v_h - v_{K^+}\|_{L^2(e)}^2 + \|\mathcal{R}_{K^-}v_h - v_{K^-}\|_{L^2(e)}^2 + \|\llbracket v_h \rrbracket\|_{L^2(e)}^2 \right) \\ &\leq Ch_e^{-2} \left(\|\mathcal{R}_{K^+}v_h - v_{K^+}\|_{L^2(K^+)}^2 + \|\mathcal{R}_{K^-}v_h - v_{K^-}\|_{L^2(K^-)}^2 \right) + h_e^{-1}\|\llbracket v_h \rrbracket\|_{L^2(e)}^2 \\ &\leq C \left(\|\nabla \mathcal{R}_{K^+}v_h\|_{L^2(K^+)}^2 + \|\nabla \mathcal{R}_{K^-}v_h\|_{L^2(K^-)}^2 + h_e^{-1}\|\llbracket v_h \rrbracket\|_{L^2(e)}^2 \right). \end{aligned}$$

For boundary faces,

$$k\|\llbracket \mathcal{R}v_h \rrbracket\|_{L^2(e)}^2 \leq C \left(kh\|\nabla \mathcal{R}_K v_h\|_{L^2(K)}^2 + k\|\llbracket v_h \rrbracket\|_{L^2(e)}^2 \right).$$

Combining these estimates and using $kh \lesssim 1$,

$$\|\mathcal{R}v_h\|_{\text{DG}}^2 \leq \sum_{K \in \mathcal{T}_h} \|\nabla \mathcal{R}v_h\|_{L^2(K)}^2 + C\|v_h\|_{\text{DG}}^2.$$

For each $K \in \mathcal{T}_h$, let v_h attain its maximum and minimum on $S(K)$ at K' and K'' , respectively. As shown in [18], for a sequence of neighboring elements $\tilde{K}_0 = K', \tilde{K}_1, \dots, \tilde{K}_M = K''$ in $S(K)$,

$$(22) \quad \|\nabla \mathcal{R}v_h\|_{L^2(K)}^2 \leq Ch^{d-2}\Lambda_m^2 \sum_{j=0}^{M-1} (v_h|_{\tilde{K}_j} - v_h|_{\tilde{K}_{j+1}})^2,$$

implying

$$(23) \quad \sum_{K \in \mathcal{T}_h} \|\nabla \mathcal{R}v_h\|_{L^2(K)}^2 \leq C \sum_{e \in \mathcal{E}_h^i} \Lambda_m^2 h_e^{-1} \|[\![v_h]\!]\|_{L^2(e)}^2.$$

Combining these bounds yields $\|\mathcal{R}v_h\|_{\text{DG}} \leq C\Lambda_m\|v_h\|_{\text{DG}}$. \square

The convergence of the iterative method is established via the Elman estimate.

Theorem 6. *Under the conditions of Lemma 6 and Lemma 7,*

$$\begin{aligned} \|P^{-1}A_\epsilon \mathbf{v}\|_P &\leq C_1 \Lambda_m^2 \|\mathbf{v}\|_P, \quad \forall \mathbf{v} \in \mathbb{C}^{n_e}, \\ |(P^{-1}A_\epsilon \mathbf{v}, \mathbf{v})_P| &\geq C_2 \frac{\epsilon}{k^2} (\mathbf{v}, \mathbf{v})_P, \quad \forall \mathbf{v} \in \mathbb{C}^{n_e}. \end{aligned}$$

Proof. From Lemma 7,

$$\begin{aligned} \|P^{-1}A_\epsilon \mathbf{v}\|_P^2 &= \mathbf{v}^* (A_\epsilon)^* P^{-1} A_\epsilon \mathbf{v} \\ &\leq (\sigma_{\max}(P^{-1/2} A_\epsilon P^{-1/2}))^2 \mathbf{w}^* \mathbf{w} \quad (\mathbf{w} = P^{1/2} \mathbf{v}) \\ &\leq C \Lambda_m^4 \mathbf{v}^* P \mathbf{v} = C \Lambda_m^4 \|\mathbf{v}\|_P^2. \end{aligned}$$

Moreover,

$$|(P^{-1}A_\epsilon \mathbf{v}, \mathbf{v})_P| = |\mathbf{v}^* A_\epsilon \mathbf{v}| \geq \frac{\epsilon}{k^2} \|[\![\mathcal{R}v]\!]\|^2 \geq C \frac{\epsilon}{k^2} \|\mathbf{v}\|_P^2.$$

This completes the proof. \square

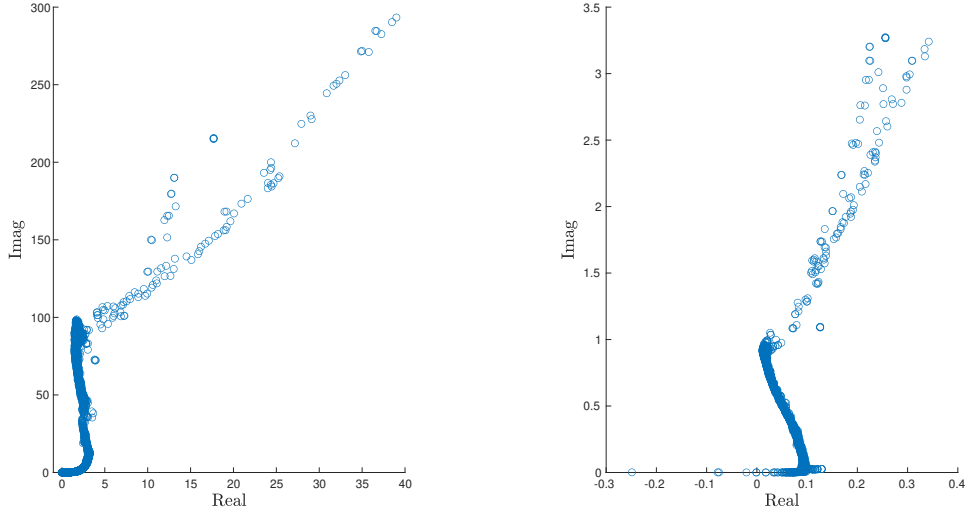
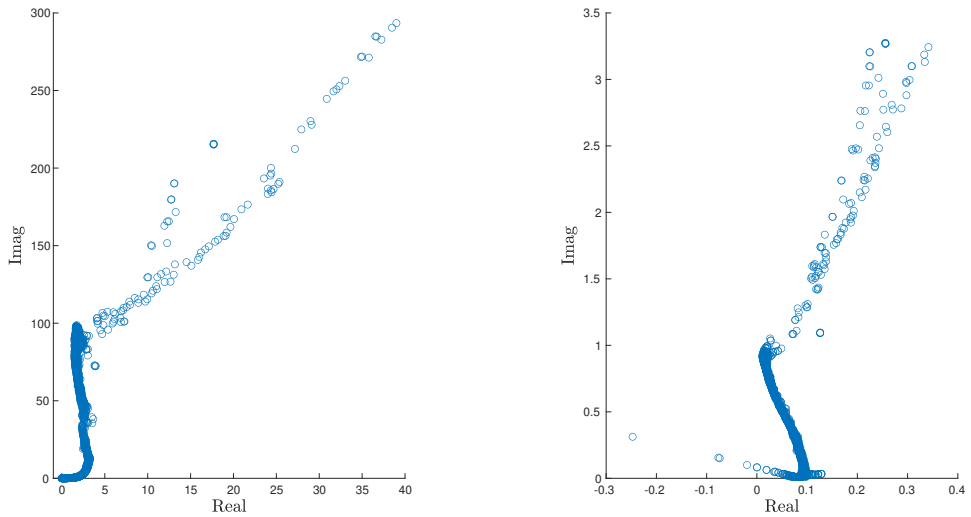
As an illustration, Figures 1 and 2 display the eigenvalues of the original and preconditioned systems on the complex plane for third-order reconstruction, with $k = 10$, for both $\epsilon = 0$ and $\epsilon = k^2$.

In each Krylov iteration, we need to compute $P^{-1}\mathbf{x}$, i.e., solve a linear system $P\mathbf{y} = \mathbf{z}$. We propose a geometric multigrid method for this purpose. Given a sequence of nested meshes $\mathcal{T}_1, \mathcal{T}_2, \dots, \mathcal{T}_r$, let U_k^0 be the piecewise constant space on \mathcal{T}_k , and P_k the discretization of $a_h^0(\cdot, \cdot)$ on $U_k^0 \times U_k^0$. Then

$$U_1^0 \subset U_2^0 \subset U_3^0 \subset \dots \subset U_r^0.$$

Define the prolongation and restriction operators as

$$\begin{aligned} I_k^{k+1} : U_k^0 &\rightarrow U_{k+1}^0, \quad I_k^{k+1} v_h = v_h, \\ I_{k+1}^k : U_{k+1}^0 &\rightarrow U_k^0, \quad I_{k+1}^k = (I_k^{k+1})^T. \end{aligned}$$

FIGURE 1. Eigenvalues for $\epsilon = 0$. Left: A_ϵ , right: $P^{-1}A_\epsilon$.FIGURE 2. Eigenvalues for $\epsilon = k^2$. Left: A_ϵ , right: $P^{-1}A_\epsilon$.

Numerical experiments confirm that this geometric multigrid solver performs well for the system $P\mathbf{y} = \mathbf{z}$.

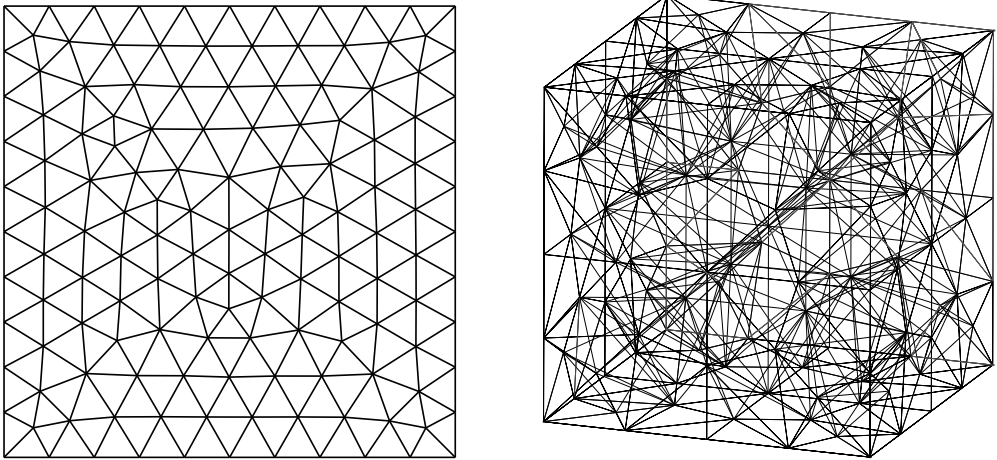


FIGURE 3. 2D triangular partition with $h = 1/10$ (left) and 3D tetrahedral partition with $h = 1/4$ (right).

5. NUMERICAL RESULTS

In this section, we perform numerical experiments to test the performance of the proposed method. We first examine the high-order convergence of the RDA space U_h^m , and then evaluate the performance of the preconditioner.

m	2	3	4	5	6
$\#S$	9	16	21	29	38

m	2	3	4
$\#S$	13	28	40

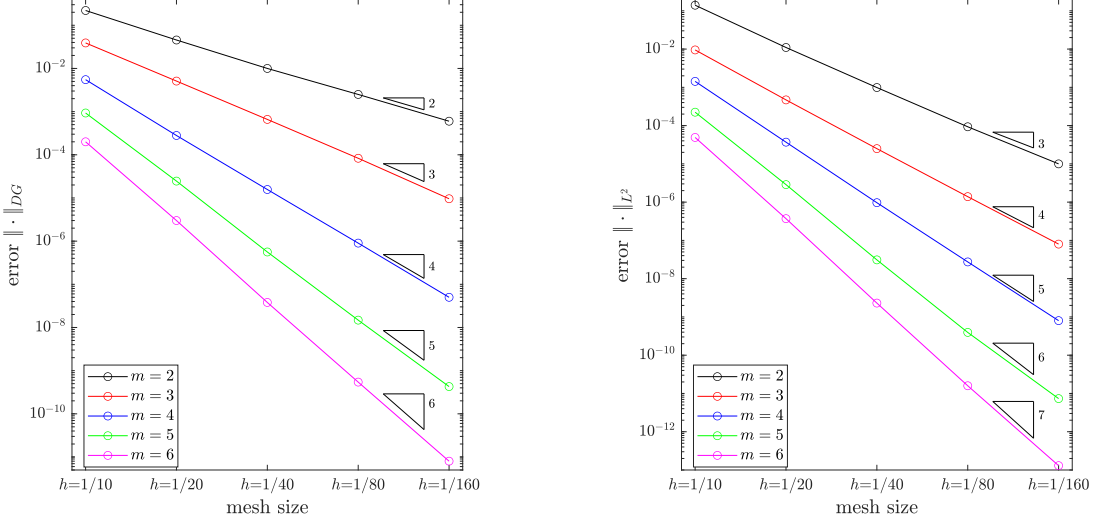
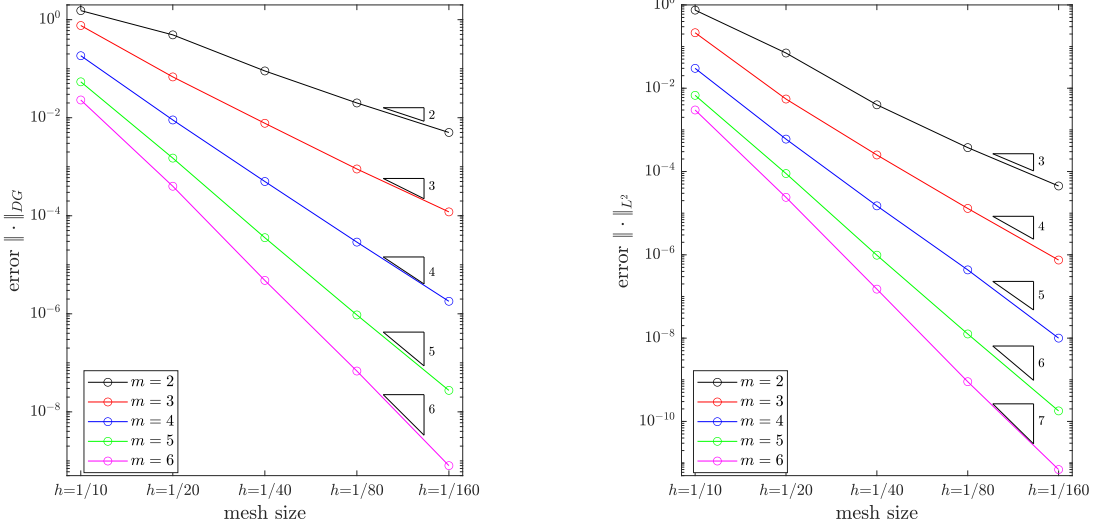
TABLE 1. The $\#S$ used in 2D and 3D examples.

Example 1 We first solve the pure Helmholtz problem on the square domain $\Omega = (0, 1)^2$, choosing the exact solution as

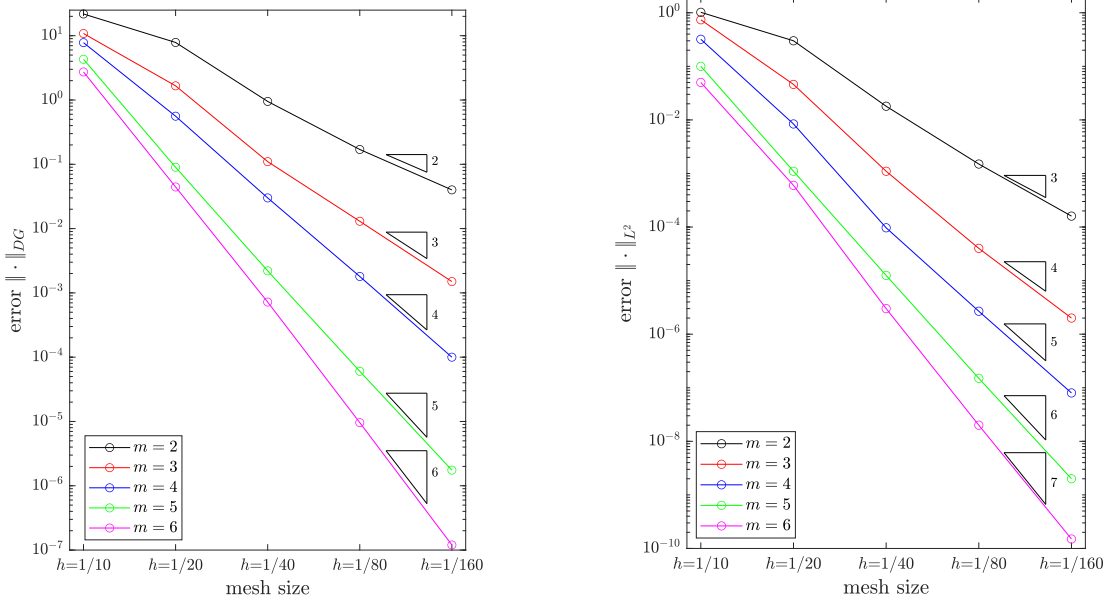
$$u(x, y) = e^{ik(x \cos \frac{\pi}{5} + y \sin \frac{\pi}{5})}.$$

We test the convergence under the norms $\|\cdot\|_{\text{DG}}$ and $\|\cdot\|_{L^2(\Omega)}$ on a series of uniformly refined meshes with $h = 1/10, 1/20, \dots, 1/160$. We consider wavenumbers $k = 5, 10, 20$ and plot the log-log errors in Figure 4, Figure 5, and Figure 6. In all experiments, we observe optimal convergence rates for the errors under both norms, which agrees with our theoretical analysis.

Example 2 We conduct a comprehensive comparative study between our proposed method and the conventional DG formulation for the Helmholtz problem. Following [15], the number of degrees of freedom in the discretized system serves as an appropriate metric for evaluating numerical efficiency. Our analysis examines the relative performance of both methodologies across a sequence of refined meshes for the case $k = 20$, with polynomial orders ranging from $2 \leq m \leq 6$. Table 2 presents the relative L^2 error ratios between the RDA and DG approaches when employing identical $\# \text{DOF}$, clearly demonstrating the

FIGURE 4. 2D accuracy test, $k = 5$.FIGURE 5. 2D accuracy test, $k = 10$.

superior efficiency of the RDA method. Figure 7 illustrates the L^2 error as a function of both the # DOF and the number of non-zero matrix entries. These results indicate that our RDA scheme achieves enhanced computational efficiency relative to the # DOF compared to standard DG implementations. Furthermore, for approximation orders $m \geq 3$, the RDA method requires fewer non-zero matrix elements than the DG counterpart to attain comparable L^2 accuracy. A more quantitative analysis is provided in Table 3, which

FIGURE 6. 2D accuracy test, $k = 20$.

details the relative ratios of # DOF and non-zero matrix entries required by the RDA method to achieve L^2 errors comparable to the DG method.

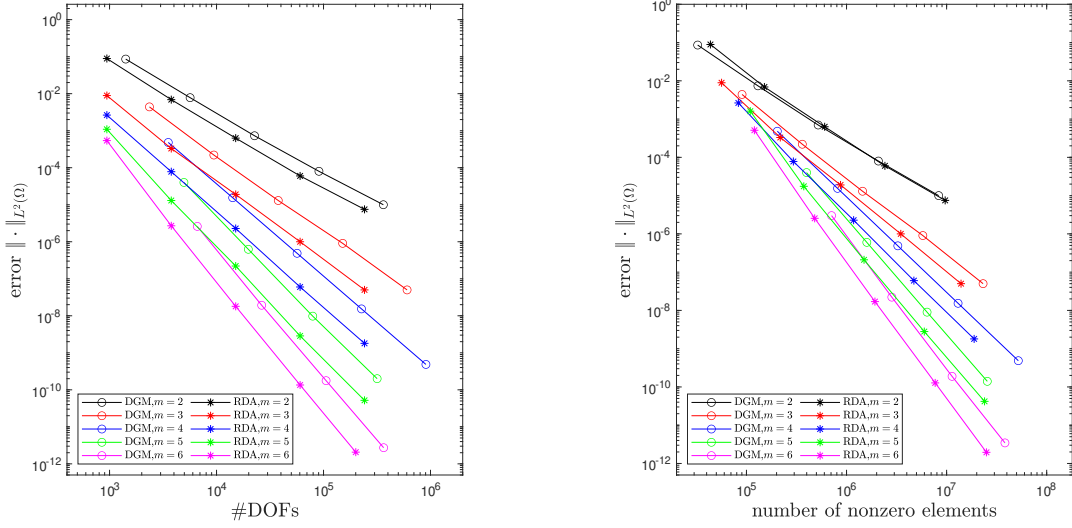


FIGURE 7. Computational efficiency comparison in two dimensions.

m	2	3	4	5	6
Relative L^2 error (RDA/DG)	0.527	0.303	0.167	0.105	0.070

TABLE 2. Relative L^2 error of the RDA method compared to the DG method using identical # DOF (Example 2).

m	2	3	4	5	6
# DOF ratio (RDA/DG)	65.6%	48.1%	38.9%	36.2%	34.3%
Non-zero entries ratio (RDA/DG)	95.5%	80.8%	70.2%	63.6%	59.8%

TABLE 3. Computational cost comparison for achieving comparable L^2 accuracy (Example 2).

Example 3 Following the methodology outlined in the preceding section, we implement the PGMRES iterative solver with P^{-1} serving as the preconditioner. Numerical experiments are conducted for both parameter configurations $\epsilon = 0$ and $\epsilon = k^2$. The solution of the auxiliary system $P\mathbf{y} = \mathbf{z}$ within each Krylov subspace iteration is computed using the geometric multigrid solver described previously. Iteration counts required for convergence across varying wavenumbers k are compiled in Tables 4, 5, and 6. The results demonstrate that employing P^{-1} as a preconditioner yields GMRES iteration counts that appear to approach a uniform upper bound as the mesh parameter h approaches zero.

m	$1/h$	10	20	40	80	160
2	48/45	46/42	45/44	44/40	41/39	
3	55/52	47/47	46/45	47/44	49/46	
4	50/49	60/58	61/59	60/56	56/52	
5	56/55	74/72	82/80	83/80	83/79	
6	81/79	88/84	100/95	114/105	125/118	

TABLE 4. Iteration counts for two-dimensional problem with $k = 5$.

To further demonstrate the computational efficiency of the proposed P^{-1} +GMG preconditioner, in Table 7 we present execution times for the GMRES method applied to the Helmholtz problem with $k = 20$. Compared to the widely used BoomerAMG preconditioner from Hypre, our P^{-1} +GMG method demonstrates superior performance in terms of both iteration counts and computational time, particularly as the mesh is refined and for higher values of m . The results consistently show that P^{-1} +GMG requires fewer iterations and significantly less CPU time across all tested configurations, with the performance gap widening as h decreases. These findings highlight the effectiveness of our preconditioner in handling Helmholtz problems with discontinuous Galerkin discretizations. The time

\diagdown m	$1/h$	10	20	40	80	160
2	67/58	76/62	77/65	77/59	75/57	
3	78/66	77/70	77/68	83/67	84/69	
4	74/68	89/79	99/87	100/85	100/82	
5	79/72	102/92	118/105	134/113	137/115	
6	103/92	122/109	142/130	221/205	262/231	

TABLE 5. Iteration counts for two-dimensional problem with $k = 10$.

\diagdown m	$1/h$	10	20	40	80	160
2	115/75	178/83	220/92	256/104	264/109	
3	180/82	205/89	216/95	266/110	273/126	
4	174/84	216/101	275/124	343/142	357/150	
5	178/96	248/125	340/138	446/180	506/190	
6	148/128	294/145	443/212	681/262	874/297	

TABLE 6. Iteration counts for two-dimensional problem with $k = 20$.

cost for the solver of traditional discontinuous Galerkin method is also provided here for reference in Table 8.

Example 4 This example demonstrates the capability of our method to handle large wavenumber problems. We solve the pure Helmholtz problem with the analytical solution given by

$$u(x, y) = \frac{\cos(kr)}{k} - \frac{\cos k + i \sin k}{k(J_0(k) + iJ_1(k))} J_0(kr), \quad r = \sqrt{(x - 0.5)^2 + (y - 0.5)^2},$$

on the unit square domain $[0, 1]^2$ with wavenumber $k = 100$. Numerical simulations are performed on an unstructured mesh with $h = 1/640$ using reconstruction order $m = 2$. Under these conditions, the PGMRES algorithm converges in 2,936 iterations with a total execution time of 5,808 seconds. Figure 8 provides a comparative visualization of the numerical solution alongside the exact solution.

Example 5 In this final example, we solve a three-dimensional Helmholtz problem defined on the cubic domain $\Omega = (0, 1)^3$, with the analytical solution specified as

$$u(x, y, z) = e^{ik(x \sin \theta \cos \phi + y \sin \theta \sin \phi + z \cos \theta)},$$

where the directional parameters are set to $\theta = \frac{\pi}{4}$ and $\phi = \frac{\pi}{5}$. Numerical tests are conducted on sequences of quasi-uniform tetrahedral meshes with $h = 1/8, 1/16, 1/32, 1/64$

m	$1/h$	10	20	40	80	160
2	$P^{-1} + \text{GMG}$	0.030 (115)	0.115 (178)	0.801 (220)	3.783 (256)	19.617 (264)
	BoomerAMG	0.024 (67)	0.265 (170)	1.945 (293)	13.119 (431)	86.027 (606)
3	$P^{-1} + \text{GMG}$	0.035 (180)	0.162 (205)	0.944 (216)	4.598 (266)	22.951 (273)
	BoomerAMG	0.049 (91)	0.518 (207)	3.412 (320)	22.568 (463)	141.721 (620)
4	$P^{-1} + \text{GMG}$	0.040 (174)	0.266 (216)	1.513 (275)	7.987 (343)	39.311 (357)
	BoomerAMG	0.079 (118)	0.785 (208)	5.296 (387)	39.943 (566)	236.073 (680)
5	$P^{-1} + \text{GMG}$	0.072 (178)	0.343 (248)	1.925 (340)	11.802 (446)	57.160 (506)
	BoomerAMG	0.114 (122)	1.215 (263)	7.946 (388)	58.290 (585)	298.676 (691)
6	$P^{-1} + \text{GMG}$	0.128 (148)	0.700 (294)	2.947 (443)	21.437 (681)	119.969 (874)
	BoomerAMG	0.194 (190)	1.993 (389)	15.980 (610)	166.05 (1085)	>300

TABLE 7. CPU time (seconds) and iteration counts (in parentheses) for GMRES with different preconditioners.

m	$1/h$	10	20	40	80
2		0.41 (176)	2.62 (210)	13.90 (282)	93.44 (383)
3		1.08 (157)	5.52 (237)	35.5 (313)	195.00 (420)
4		2.23 (198)	13.41 (272)	79.46 (350)	>300
5		5.52 (216)	36.74 (269)	196.03 (416)	>300
6		12.66 (368)	84.45 (456)	>300	> 300

TABLE 8. CPU time cost for DG method with BoomerAMG preconditioner.

for wavenumber $k = 8$. Figure 9 displays the convergence behavior under both L^2 and energy norms, confirming the theoretical convergence rates.

Following the methodology of Example 2, we extend our analysis to include a comprehensive efficiency comparison in three dimensions. This comparison examines the trade-off between computational cost and numerical accuracy, with detailed results summarized in Table 9 and Table 10. The comparative data is graphically illustrated in Figure 10, demonstrating that the RDA method requires significantly fewer # DOF and non-zero matrix elements than the traditional DG approach, particularly for higher approximation orders.

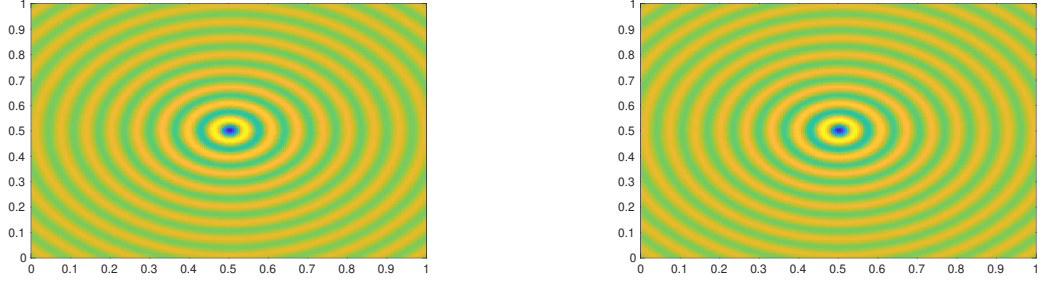
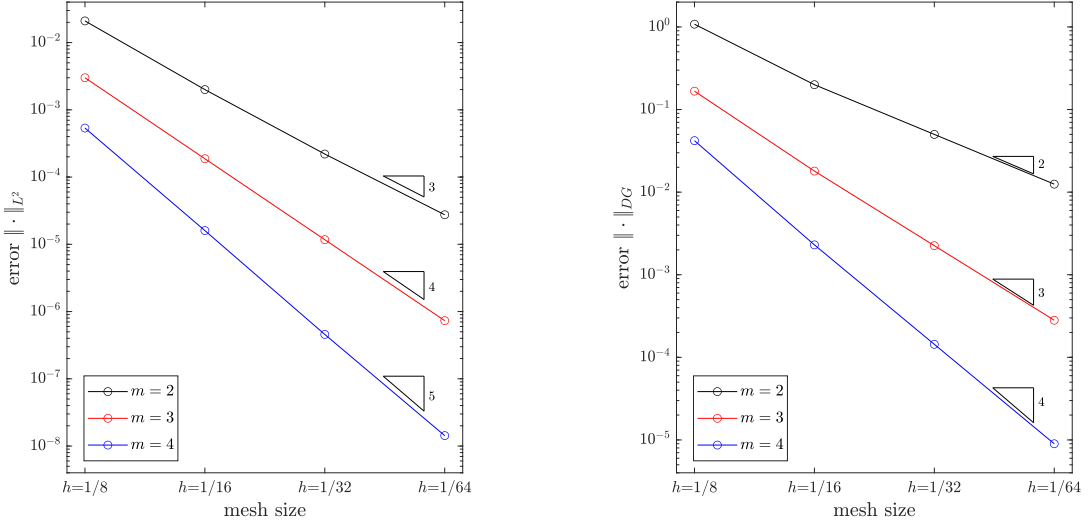


FIGURE 8. Numerical solution (left) and exact solution (right).

The performance of the preconditioner P^{-1} in three dimensions is documented in Table 11. Notably, the iteration counts remain uniformly bounded with respect to mesh refinement for both parameter configurations ($\epsilon = 0$ and $\epsilon = k^2$), underscoring the robustness and scalability of our preconditioning strategy.

FIGURE 9. Three-dimensional accuracy test, $k = 8$.

m	2	3	4
Relative L^2 error (RDA/DG)	0.501	0.245	0.084

TABLE 9. Relative L^2 error of the RDA method compared to the DG method using identical # DOF (Example 5).

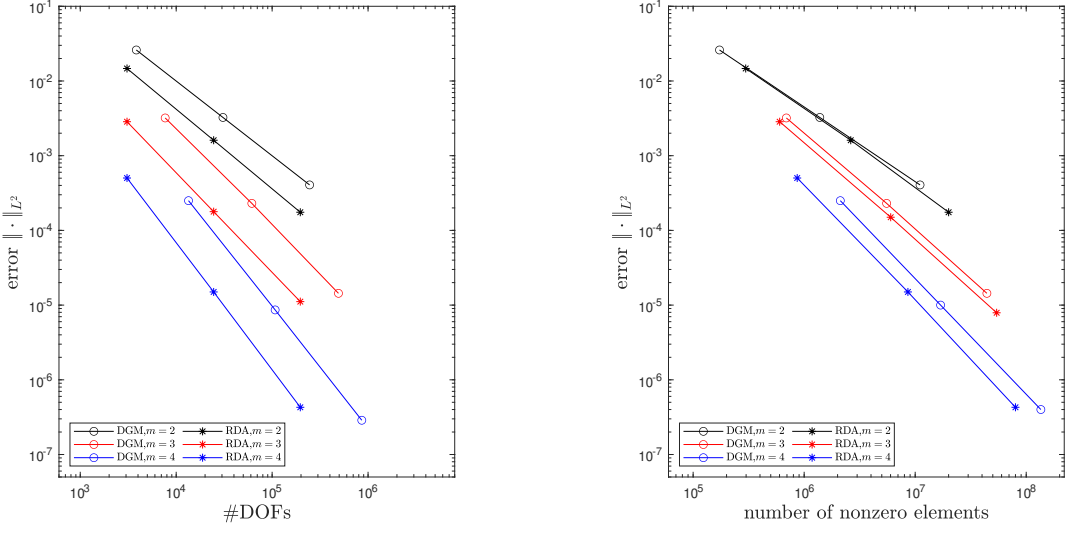


FIGURE 10. Computational efficiency comparison in three dimensions.

m	2	3	4
# DOF ratio (RDA/DG)	49.8%	32.6%	23.2%
Non-zero entries ratio (RDA/DG)	83.2%	68.1%	44.6%

TABLE 10. Computational cost comparison for achieving comparable L^2 accuracy in three dimensions (Example 5).

m	$1/h$	8	16	32	64
2		135/116	144/135	147/139	155/142
3		128/105	148/112	164/153	177/160
4		125/132	172/165	248/194	279/219

TABLE 11. Iteration counts for three-dimensional problem with $k = 8$.

6. CONCLUSION

In this paper, we have developed and analyzed an efficient solver for the Helmholtz equation based on a novel approximation space. The proposed method demonstrates superior performance over traditional approaches, achieving higher accuracy with reduced

degrees of freedom and lower memory requirements. By incorporating a natural preconditioner through piecewise constant discretization, the method also significantly reduces computational time. Numerical experiments in both 2D and 3D confirm its effectiveness.

ACKNOWLEDGEMENTS

The authors would like to thank Professor Ruo Li from Peking University and Fanyi Yang from Sichuan University for their valuable suggestions and advice, which have significantly improved the quality of this manuscript. This research was supported by the High-performance Computing Platform of Peking University.

REFERENCES

1. S. Congreve, J. Gedcke, and I. Perugia, *Robust adaptive hp discontinuous Galerkin finite element methods for the Helmholtz equation*, SIAM J. Sci. Comput. **41** (2019), no. 2, A1121–A1147. MR 3937921
2. Songyao Duan and Haijun Wu, *Adaptive fem for helmholtz equation with large wavenumber*, Journal of Scientific Computing **94** (2022).
3. Y. A. Erlangga, C. Vuik, and C. W. Oosterlee, *On a class of preconditioners for solving the helmholtz equation*, Applied Numerical Mathematics **50** (2004), no. 3, 409–425.
4. ———, *A novel multigrid based preconditioner for heterogeneous helmholtz problems*, SIAM Journal on Scientific Computing **27** (2006), 1471–1492.
5. C. Farhat, I. Harari, and U. Hetmaniuk, *A discontinuous Galerkin method with Lagrange multipliers for the solution of Helmholtz problems in the mid-frequency regime*, Comput. Methods Appl. Mech. Engrg. **192** (2003), no. 11-12, 1389–1419.
6. X. Feng and H. Wu, *Discontinuous Galerkin methods for the Helmholtz equation with large wave number*, SIAM J. Numer. Anal. **47** (2009), no. 4, 2872–2896.
7. ———, *hp -discontinuous Galerkin methods for the Helmholtz equation with large wave number*, Math. Comp. **80** (2011), no. 276, 1997–2024.
8. M. Gander, I. Graham, and E. Spence, *Applying gmres to the helmholtz equation with shifted laplacian preconditioning: what is the largest shift for which wavenumber-independent convergence is guaranteed?*, Numerische Mathematik **131** (2015), 567–614.
9. S. Gong, I. Graham, and E. Spence, *Domain decomposition preconditioners for high-order discretizations of the heterogeneous helmholtz equation*, IMA Journal of Numerical Analysis **41** (2021), 2139–2185.
10. ———, *Convergence of restricted additive schwarz with impedance transmission conditions for discretised helmholtz problems*, Mathematics of Computation **92** (2023), 175–215.
11. I. Graham, E. Spence, and E. Vainikko, *Domain decomposition preconditioning for high-frequency helmholtz problems with absorption*, Mathematics of Computation **86** (2015), 2089–2127.
12. I. Graham, E. Spence, and J. Zou, *Domain decomposition with local impedance conditions for the helmholtz equation with absorption*, SIAM Journal on Numerical Analysis **58** (2020), 2515–2543.
13. R. H. W. Hoppe and N. Sharma, *Convergence analysis of an adaptive interior penalty discontinuous Galerkin method for the Helmholtz equation*, IMA J. Numer. Anal. **33** (2013), no. 3, 898–921. MR 3081488
14. Q. Hu and R. Song, *A novel least squares method for Helmholtz equations with large wave numbers*, SIAM J. Numer. Anal. **58** (2020), no. 5, 3091–3123.
15. T. J. R. Hughes, G. Engel, L. Mazzei, and M. G. Larson, *A comparison of discontinuous and continuous Galerkin methods based on error estimates, conservation, robustness and efficiency*, Discontinuous Galerkin methods (Newport, RI, 1999), Lect. Notes Comput. Sci. Eng., vol. 11, Springer, Berlin, 2000, pp. 135–146.
16. F. Ihlenburg and I. Babuška, *Finite element solution of the Helmholtz equation with high wave number. I. The h -version of the FEM*, Comput. Math. Appl. **30** (1995), no. 9, 9–37.
17. ———, *Finite element solution of the Helmholtz equation with high wave number. II. The h - p version of the FEM*, SIAM J. Numer. Anal. **34** (1997), no. 1, 315–358.

18. R. Li, Q. Liu, and F. Yang, *Preconditioned nonsymmetric/symmetric discontinuous Galerkin method for elliptic problem with reconstructed discontinuous approximation*, accepted by J. Sci. Comput. (2023).
19. R. Li, P. Ming, Z. Sun, and Z. Yang, *An arbitrary-order discontinuous Galerkin method with one unknown per element*, J. Sci. Comput. **80** (2019), no. 1, 268–288.
20. R. Li, P. Ming, and F. Tang, *An efficient high order heterogeneous multiscale method for elliptic problems*, Multiscale Model. Simul. **10** (2012), no. 1, 259–283.
21. R. Li and F. Yang, *A reconstructed discontinuous approximation to Monge-Ampère equation in least square formulation*, Adv. Appl. Math. Mech. **15** (2023), no. 5, 1109–1141. MR 4613677
22. P. Lu, X. Xu, B. Zheng, and J. Zou, *Two-level hybrid schwarz preconditioners for the helmholtz equation with high wave number*, submitted (2024).
23. J. M. Melenk and S. Sauter, *Wavenumber explicit convergence analysis for Galerkin discretizations of the Helmholtz equation*, SIAM J. Numer. Anal. **49** (2011), no. 3, 1210–1243.
24. N. C. Nguyen, J. Peraire, F. Reitich, and B. Cockburn, *A phase-based hybridizable discontinuous Galerkin method for the numerical solution of the Helmholtz equation*, J. Comput. Phys. **290** (2015), 318–335.
25. L. L. Thompson and P. M. Pinsky, *A Galerkin least-squares finite element method for the two-dimensional Helmholtz equation*, Internat. J. Numer. Methods Engrg. **38** (1995), no. 3, 371–397.

INSTITUTE OF APPLIED PHYSICS AND COMPUTATIONAL MATHEMATICS, BEIJING 100094, P.R. CHINA
 Email address: shuhai@pku.org.cn